Journal Name

ARTICLE

Chirality as a tool for function in porous organic cages

Received 00th January 20xx,
Accepted 00th January 20xx

DOI: 10.1039/x0xx00000x

www.rsc.org/

T. Hasell,[a]* M. A. Little,[a] S. Y. Chong,[a] M. Schmidtmann,[b] M. E. Briggs,[a] V. Santolini,[c] K. E. Jelfs,[c] and A. I. Cooper[a]*

The control of solid state assembly for porous organic cages is more challenging than for extended frameworks, such as metal-organic frameworks. Chiral recognition is one approach to achieving this control. Here we investigate chiral analogues of cages that were previously studied as racemates. We show that chiral cages can be produced directly from chiral precursors or by separating racemic cages by co-crystallisation with a second chiral cage, opening up a route to producing chiral cages from achiral precursors. These chiral cages can be cocrystallized in a modular, 'isoreticular' fashion, thus modifying porosity, although some chiral pairings require a specific solvent to direct the crystal into the desired packing mode. Certain cages are shown to to interconvert chirality in solution, and the steric factors governing this behavior are explored both by experiment and by computational modelling.

Introduction

Microporous materials have potential applications in gas storage, separation, and heterogeneous catalysis.[1] Most microporous solids are extended networks, such as metal-organic frameworks (MOFs),[2] covalent organic frameworks (COFs),[3] or organic polymer networks.[4] However, there is also growing interest in porous molecular solids, such as porous organic cages.[5-7] These cages comprise an internal void, open windows, and a rigid structure that prevents collapse, thus allowing accessible porosity to guest molecules. Porous organic cages have been prepared using imine condensation,[8-11] boronic ester formation,[12] and direct carbon-carbon bond-forming reactions.[13] Molecular cage materials with apparent Brunauer–Emmett–Teller (BET) surface areas as high as 3758 $m^2 g^{-1}$ have been prepared.[14] Since cages are discrete molecules, they are soluble in common organic solvents and can be processed into support materials or crystallized into the solid state, as required. We previously reported a class of porous [4+6] cycloimine cage compounds (Fig. 1).[8, 15] The gas sorption properties of these cages depend both on the structure of the cage itself and on its crystal packing, with multiple polymorphs being possible for most cages.[15, 16] Helicity, or axial chirality, is an intrinsic property of this family of cages (Fig. 1). This chirality is significant because it plays an important role in controlling the crystalline assembly of these molecules.

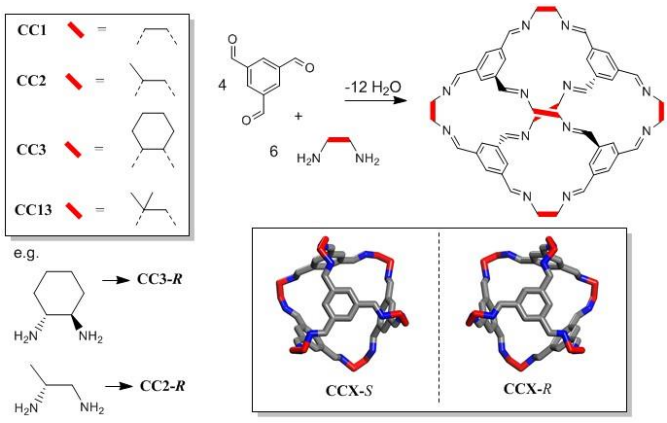

Figure 1. Chemical structure and synthesis of a range of tetrahedral 4+6 imine bonded covalent cages. Lower right inset illustrates helical chirality.

Cages of opposite chirality are often found to pack more closely, thus forming a preferred, lower energy packing. This has been observed not only for [4+6] imine cage structures, as shown in Fig. 1,[8] but also [3+6] tubular imine based cages[17] and [2+3] salicylimine cages.[18] This strong chiral recognition allows different cages to be combined in a modular fashion to produce cocrystals by design. Hence, the properties of the resultant cocrystals can be tailored by the choice of the substituents on the cage building blocks. Chiral interactions can also be used to control the size and shape of the cage crystals,[19] and even to produce ternary cocrystals containing three different cage molecules.[20] The chirality of the cages also allows selective

[a] Univ Liverpool, Dept Chem, Crown St, Liverpool L69 7ZD, Merseyside, England.
[b] Institut für Chemie, Universität Oldenburg, Carl-von-Ossietzky-Straße 9 – 11 26129 Oldenburg
[c] Imperial Coll London, Dept Chem, London SW7 2AZ, England.
† Footnotes relating to the title and/or authors should appear here.
Electronic Supplementary Information (ESI) available: [details of any supplementary information available should be included here]. See DOI: 10.1039/x0xx00000x

binding of chiral organic guest molecules such as 1-phenylethanol, thus allowing applications in enantioselective separation.[21-25]

Some cages have been studied as both their chiral and racemic forms, which can have different crystal packings and physical properties.[19] However, cages **CC2** and **CC13** (Fig. 1) have only previously only been reported as racemates. We therefore set out to isolate both cages as homochiral materials, since this should allow new properties and opportunities for new cocrystal combinations.

RESULTS AND DISCUSSION

Direct synthesis of chiral CC2

We previously reported **CC2** in its racemic form, and showed that it can exist as more than one racemic polymorph.[8, 15] Initial attempts to synthesize **CC2** from its commercially-available homochiral diamine following the same protocol used for its racemic form[8] failed due to the catenation (interlocking) of the cages.[26] The standard synthesis for **CC2** is to layer the aldehyde and amine and allow them to mix slowly, forming crystals of cage over 1–2 weeks that can then be isolated by filtration. Slow mixing of the precursors encourages the formation of discrete cages, rather than polymeric by-products.[9] For racemic **CC2**, the formation of catenated cages, which we believe to be the thermodynamic product, requires either long equilibration times (months) or acid catalysts (trifluoroacetic acid).[26] However, for chiral **CC2**, the products are a mixture of monomeric and catenated cages after only a few days, and after the standard reaction time for racemic **CC2** (1 week), chiral **CC2** forms the catenane exclusively (Fig. S1). The chirality of the cage is important in this process. For racemic **CC2**, cages always 'self sort' to form catenanes comprised of two cages of the same chirality. This is because cages of equivalent helicity are needed for interlocking since opposite chirality would result in unfavorable close contacts.[26] Hence, for the racemate to form catenated **CC2** cages, each catenane must select 12 diamines of a single chirality from the racemic mixture. There is no such requirement for self-sorting in the chiral **CC2** case, which rationalizes the greatly increased rate of catenation that we observe. To overcome this, the synthesis method was adapted to a high dilution dropwise addition of diamine to tri-aldehyde with stirring, with product isolation by rotary evaporation after only 24 hours. In this case, unwanted polymer formation was discouraged by the high dilution and slow reagent addition, while the mixing and short reaction time allowed monomeric cages to be produced as the kinetic product before catenanes could form. The structure and physical properties of chiral **CC2** from direct synthesis were identical to those of chiral **CC2** formed by separation, as described below.

Chiral CC2 separated by co-crystallisation

Previously, we showed that the chirality of racemic **CC1** can be resolved by homochiral **CC3**-*R* via the formation of a (**CC3**-*R*, **CC1**-*S*) quasiracemic cocrystal.[27] In that system, **CC1** is flexible and its helical chirality can interconvert in solution.[28] Hence, when **CC3**-*R* is crystallised in a 1:1 ratio with **CC1**, a cocrystal is formed in 100% yield where all the **CC1** component has *S* chirality. By contrast, the more sterically hindered structure of **CC2** (Fig. 1) cannot interconvert helical chirality in solution. We therefore hypothesized, by analogy, that a (**CC3**-*R*, **CC2**-*S*) cocrystal might be formed if racemic **CC2** were mixed with homochiral **CC3**-*R* in a 2:1 ratio, leaving the **CC2**-*S* component excluded in solution (Fig. 2). This prove to be the case: when racemic **CC2** and **CC3**-*R* were co-crystallised together, quasiracemic (**CC3**-*R*, **CC2**-*S*) cocrystals were isolated, which could be separated from the **CC2**-*R*, which remained in solution, by simple filtration (ESI, Figs S2, S3).

In the crystal structure of (**CC3**-*R*, **CC2**-*S*), the cage molecules pack window-to-window to generate a 3-D diamondoid pore structure running throughout the crystals (Fig. 3). There is a clear trend in powder XRD patterns of different cages and cage combinations that adopt this isostructural, diamondoid packing mode (Fig. 4).

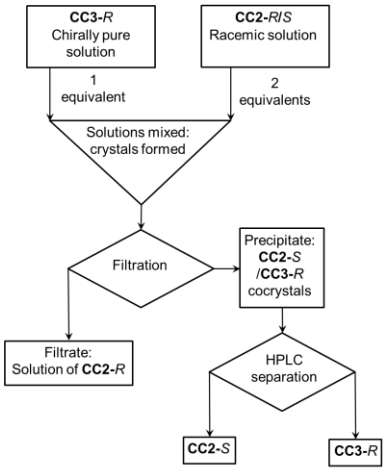

Figure 2. Schematic representation of the process of cage separation by chiral co-crystallisation.

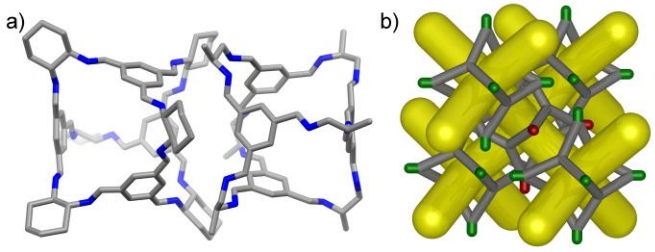

Figure 3. a) The heterochiral window-to-window interaction in the (**CC2**-*R*/**CC3**-*S*) crystal structure and b) a schematic representation of the packing (**CC2** and **CC3** shown with green and red vertices, respectively), showing the diamondoid pore network (yellow).

As the cages become smaller, with less sterically bulky vertices, they can pack closer together and the diffraction patterns shift to higher angles due to the smaller crystal repeat. Also, when moving from a homochiral to a heterochiral system, the cages

can pack more efficiently. The cage–cage distances, and hence the unit cell dimensions, fall in the following order: homochiral **CC3** > heterochiral **CC3** > heterochiral **CC2**/**CC3** > heterochiral **CC2** (Fig. 4b). Gas sorption measurements for the heterochiral **CC2**/**CC3** quasiracemic cocrystal show that its porosity also follows the trend that would be expected from an expansion in the unit cell (Fig. 5). The nitrogen uptake of the heterochiral (**CC3**-*R*, **CC2**-*S*) cocrystal falls between that of racemic **CC3** and racemic **CC2**β (the β phase packs in the equivalent window-window packing mode).[15]

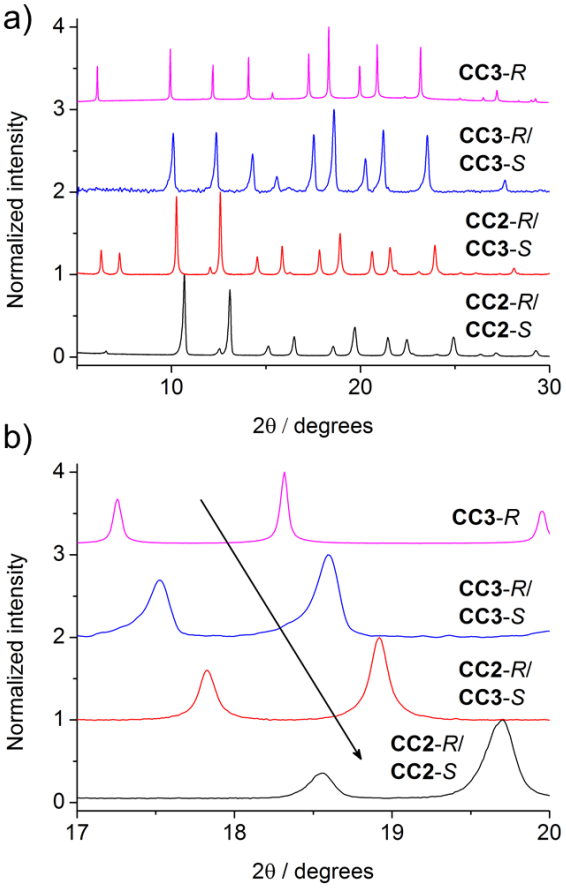

Figure 4. PXRD patterns of cage crystals and cocrystals. a) The similarity in powder patterns across the systems is indicative of their isoreticular structures. b) The shift of peaks to the right (smaller unit cells) can be observed when going from a homochiral to racemic system, and as **CC3** is replaced with the smaller **CC2**.

It is likely that defects induced by rapid crystallization also contribute to the porosity of the crystal, since we previously found that more rapid precipitation induces higher porosity.[19] When opposite chiralities of **CC3** are mixed, the dramatic decrease in solubility causes very rapid precipitation. By comparison, the higher solubility of **CC2** leads to slower precipitation of cocrystals, and likely fewer defects.[15]

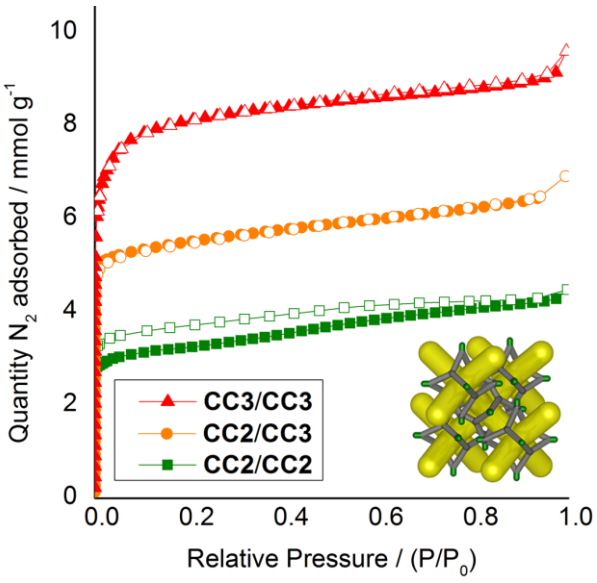

Figure 5. Nitrogen sorption isotherms (77 K, 1 bar) for racemic and quasiracemic crystals and cocrystals of **CC2** and **CC3,** all assembled in a diamondoid window-window packing mode (inset)**. CC2** racemate, green squares; (**CC2**/**CC3**) cocrystal quasiracemate orange circles, and; **CC3** racemate red triangles. Adsorption isotherms shown as solid symbols; desorption curves as open symbols.

The physical properties of homochiral **CC2**, made by both direct synthesis and separation by co-crystallisation, were investigated with respect to racemic **CC2**. Homochiral **CC2** is approximately 3 times more soluble than the **CC2** racemate (~600 vs. ~200 mg/mL in chloroform). Given that applications of these porous materials might exploit their solution processability,[5] this could provide a practical advantage. Homochiral **CC2** also displays contrasting crystallization behavior to the racemate. A previous study found that racemic **CC2** formed crystalline phases from all 40 solvent systems tested, most forming the α-phase that hash 1-dimensional pore channels running between the cages.[15] By contrast, crystallization with 1,4-dioxane afforded a window-to-window-packed β-phase with a 3-D diamondoid pore network.[15] Homochiral **CC2** exhibits a lower propensity to crystallize, as indicated by its higher solubility, and forms an amorphous phase from many solvent systems (Fig. S4). However, several crystallisation solvents did generate ordered materials. Notably, 1,4-dioxane produced a homochiral solvate structure that was markedly different from the window-to-window structure observed for racemic **CC2** (Fig. 6).[15] In the **CC2**-*R* dioxane solvate there are no window-to-window interactions between cages; instead, the cages pack window-to-vertex and window-to-arene (Fig. 6). A mixture of ordered, and disordered 1,4-dioxane molecules occupy the cage cavities and interstitial lattice sites between inefficiently packed cages. Unsurprisingly, this structure is not stable to desolvation, but it highlights the marked difference in crystallisation behavior between chiral and racemic forms of the same cage. Some solvents tested produce PXRD patterns that suggest a packing mode that is analogous to the **CC2** racemate α-phase, with 1-dimensional

inter-cage channels. Crystallization with one such solvent, *m*-xylene, was scaled up to allow characterisation by single crystal X-ray diffraction (SCXRD) and gas sorption analysis (Fig. 7, 8, and S5). The sorption isotherms show that chiral **CC2** has a lower nitrogen uptake than racemic **CC2** when they adopt the same α-packing mode (apparent BET surface areas of 307 and 532 $m^2 g^{-1}$, respectively). We previously investigated whether the internal cavities of the **CC2** cages are accessible to gases, or if diffusion is restricted to the 1-dimensional channel running between the cages.[8, 29] These results suggest that the accessibility of the cage cavities to nitrogen is dependent on the chirality of the structure: that is, open in the case of the racemic **CC2** crystals but closed in the homochiral form.

Chiral CC13 separated by co-crystallisation

CC13 (Figure 1) was previously reported as a racemate,[15] which was shown to have both the highest surface area and the highest solubility of any of the [4+6] cages based on 1,3,5-triformylbenzene.[15] By analogy with **CC2**, separation of **CC13** into its enantiomerically-pure forms, might improve the solubility and, potentially, the porosity even further. Unlike **CC2**, is not possible to synthesize homochiral **CC13** directly from chiral precursors because the diamine precursors themselves are achiral.

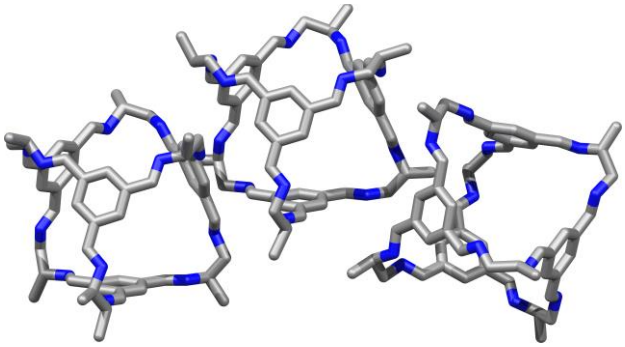

Figure 6. Single crystal structure of the homochiral **CC2**-*R* 1,4-dioxane solvate **CC2**-*R*·4.5(1,4-dioxane)·4.25(H_2O), showing window-to-vertex packing (left), and window-to-arene packing (right).

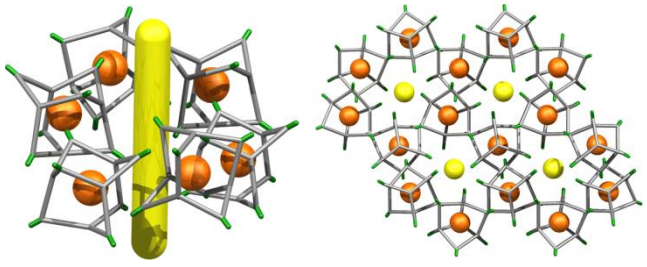

Figure 7. Crystal packing of **CC2**-*R* molecules in the single crystal structure **CC2**-*S*·*1.7(m*-xylene). 1-D extrinsic voids (yellow line) are located between hexagonally arranged stacks of **CC2**-*R* molecules.

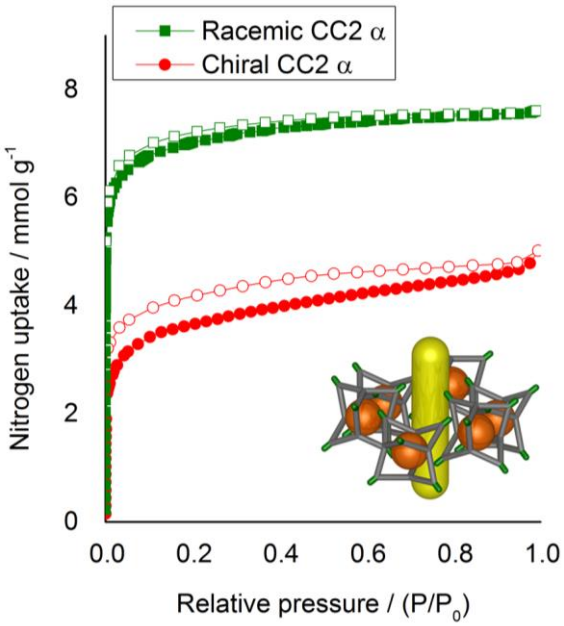

Figure 8. Nitrogen sorption isotherms (77 K, 1 bar) for racemic and homochiral **CC2,** in the 1-dimensional inter-cage channel packing mode. Homochiral **CC2**, red circles. Racemic **CC2**, green squares. Adsorption isotherms shown as solid symbols, and desorption curves as open symbols.

This leaves chiral separation of the racemate into its constituent helical enantiomers as the only potential route to the chiral form of **CC13**. Separation of the **CC13** racemate by co-crystallisation with **CC3** was therefore attempted, following the same methodology validated for **CC2**.

When racemic **CC13** and **CC3**-*R* were mixed in a 2:1 ratio in CH_2Cl_2/2-propanol, a cocrystal was formed (Fig. 9, S6) with the two cage molecules in the desired 1:1 composition. Surprisingly, however, the expected window-to-window packing mode did not occur, but rather an arene-to-window packing was observed that was reminiscent of **CC2**-α (Fig. 9a). This is notable since all previous cocrystals in this cage [4+6] family show a strong preference for the window-to-window form.[17, 19, 27] More surprisingly, and contrary to the **CC2** case, this **CC3/CC13** cocrystal selects cages of the same chirality: that is, **CC3**-*R* pairs with **CC13**-*R*. In the crystal structure, 2D networks of window-to-arene packed cages are stacked along the crystallographic *c* axis (Figure 9b & c). The two novel aspects of this cage cocrystal system—the non-window packing and the selection of a single chirality—are likely correlated. The previously observed tendency of this family of cages, to form pseudoracemic cocrystals[20, 27] is therefore a function of the specific window-to-window interaction and is not generalizable to all analogues. This (**CC3**-*R*, **CC13**-*R*) cocrystal is less desirable in terms of porosity and it also showed poor stability to desolvation.

As described previously, [15] 1,4-dioxane can act as a directing agent to direct racemic cages to pack window-to-window, even for cages where this would not ordinarily be the lowest energy polymorph.[15] This technique proved transferable to the (**CC3**-

R, **CC13**-*R*) system, which was directed to pack window-to-window (Fig. 10). When **CC3**-*R* and **CC13** were crystallized from a CH_2Cl_2/1,4-dioxane solution, single crystals of **CC3**-*R*·0.65(**CC13**-*S*)·0.35(**CC13**-*R*)·1.96(1,4-dioxane)·2.25(CH_2Cl_2)·6(H_2O) were isolated. SCXRD showed that the expected 1:1 cocrystal was formed, with **CC3**¬*R* and **CC13** occupying separate crystallographic sites. However, the **CC13** site is disordered, with occupancies of 65 % and 35 % for the *S*- and *R*-enantiomers, respectively. On sites occupied by **CC13**-*S*, the cages form the heterochiral window-to-window packing motif with adjacent **CC3**-*R* cages, with 1,4-dioxane located in the window cavities (Fig. 10). In contrast, when **CC13**-*R* is present, the cage is oriented to form window-to-arene interactions with its **CC3** neighbors, as is observed in (**CC3**-*R*/**CC13**-*R*), rather than forming a homochiral **CC3**—**CC13** window-to-window motif. For simplicity, if we consider **CC13**-*S* to occupy all **CC13** sites in the crystal lattice, each **CC3**-*R* molecule packs in a window-to-window arrangement with three **CC13**-*S* cage molecules. This propagates 2-D hexagonal layers in the *ab* plane that pair with an adjacent layer *via* window-to-window interactions between **CC3**-*R* molecules, which bridge the two networks (Fig. 11b). These double layers stack along the *c*-axis (Fig. 11c), with CH_2Cl_2 molecules filling the space in between. For the predominant **CC3**—**CC13** window-to-window interaction, the pairing of cages of opposing chiralities is once again observed, providing that 1,4-dioxane crystallises in the window site in 65% of the crystal structure.

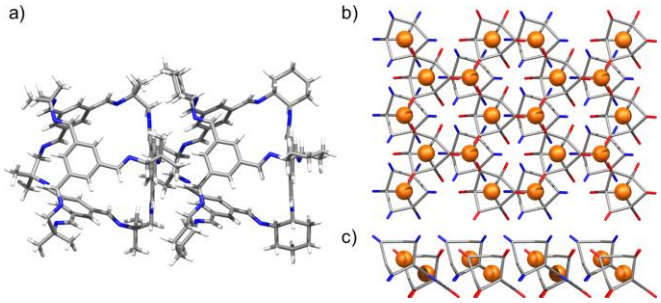

Figure 9. Single crystal structure of **CC3**-*R*·**CC13**-*R*·6(2-propanol)·CH_2Cl_2·4(H_2O) displaying **CC3**-*R* window to **CC13**-*R* arene packed cages (a), propagating a 2-D network structure of window-to-arene packed **CC3**-*R* (red) and **CC13**-*R* (blue) cages; perspective view [001] (b), and [010] (c).

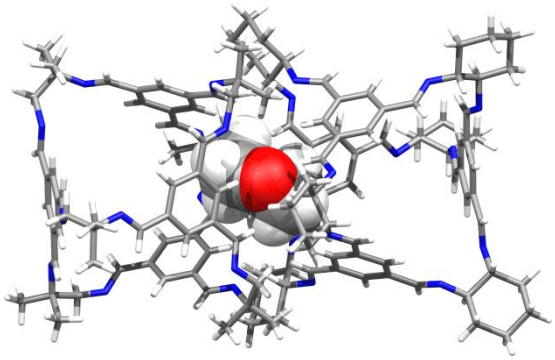

Figure 10. 1,4-Dioxane directed window-to-window pairing of **CC3**-*R*/**CC13**-*S* from the single crystal structure **CC3**-*R*·0.65(**CC13**-*S*)·0.35(**CC13**-*R*)·1.96(1,4-dioxane)·2.25(CH_2Cl_2)·6(H_2O).

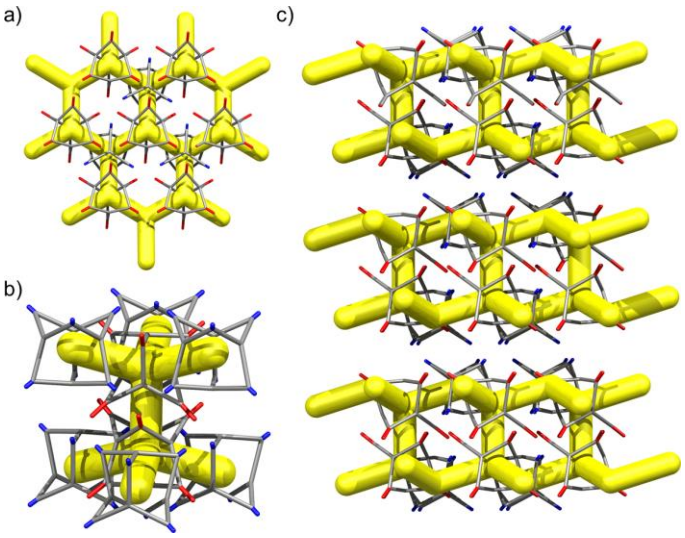

Figure 11. Representation of the single crystal structure **CC3**-*R*·0.65(**CC13**-*S*)·0.35(**CC13**-*R*), only **CC13**-*S* is shown. Window-to-window packing between **CC3**-*R* (red) and **CC13**-*S* (blue) propagates a 2-D network structure (a). Two hexagonal 2-D networks of **CC3**-*R*-**CC13**-*S* are connected by window-to-window packed **CC3**-*R* cages (b), that are staggered along *c* (c).

This predominantly window-to-window (**CC3**, **CC13**) cocrystal retains crystallinity on desolvation (Figs. S7, S8). In contrast to **CC2**/**CC3**, this structure does not exhibit sorption behavior that is intermediate between that of its respective parent cages (Fig. 11). Racemic **CC13**, when packed window-to-window, was shown before to possess a second 3-D pore network,[15] formed from a series of connected extrinsic cavities present outside of the cages. This second network forms because the dimethyl vertices of **CC13** push the cages apart and open up additional free volume.[15] By contrast, when **CC13** is co-crystallized with **CC3**, this additional pore network is blocked by the cyclohexane vertices of **CC3**, dramatically reducing the porosity to nitrogen for in the **CC3**/**CC13** cocrystals with respect to racemic **CC13** (Fig. 12). There is also a small difference in packing between crystals of racemic **CC3** and those of **CC3**/**CC13** (Fig. 11b). The layered structure of **CC3**/**CC13** means that although most cage windows face the window of an adjacent cage, a small proportion (approximately 1/3) face instead into three cage vertices of the opposing layer. This reduces the porosity of those window sites, slightly reducing the overall uptake in comparison to racemic **CC3** (Fig. 12). Sorption of additional gases is reported in Fig. S9.

After removal of the cocrystalline **CC3**-*R*/**CC13**-*R* precipitate, the residual cage present in the filtrate was crystallized. However, SCXRD structural determination revealed the resultant material to be racemic **CC13**, rather than the expected homochiral form. Racemic material was also obtained after separation of **CC13** from the cocrystal by HPLC. Since the **CC13** in the cocrystal was shown to be homochiral, this suggests that **CC13** can interchange chirality in solution, and revert to a racemic mixture. Variable temperature NMR confirmed that at <203 K the vertex protons of **CC13** are resolved, but that they are merged at higher temperatures, indicating that this chiral

exchange occurs rapidly at room temperature in solution (Figs. 13, S10). Chiral interconversion has been previously documented for **CC1**.[28] However, interconversion does not occur for **CC2**, even in solution. There is a clear progression in the steric demand of the vertex groups from **CC1** (non-functionalised vertices) to **CC2** (methyl functionalised vertices) to **CC13** (dimethyl functionalised vertices). Why, then, do the single methyl groups of **CC2** act to prevent interconversion while the dimethyl groups of **CC13** allow it? The methyl groups of **CC2** have been shown to exclusively occupy the *exo* position (away from the cage) in preference to the *endo* position (towards the cage) (Fig. 14).[26] Therefore, for **CC2**-*R* (formed with all methyl groups in the more favorable *exo* position) to 'flip' chirality to *S* requires six methyl groups to occupy the unfavorable *endo* position. This is not the case for **CC1**, as it has no sterically unfavorable methyl-cage contacts. Nor is it the case for **CC13**, because this cage must have an unfavorable methyl-cage contact for either enantiomer. This unfavorable repulsion of the methyl group from the cage may contribute to the lower activation energy for the chiral interconversion of **CC13** in comparison to **CC1** (24 and 35 kJ mol^{-1}, respectively), as the energy well at either side of the barrier to conversion for **CC13** would be expected to be shallower. Therefore, while **CC1** and **CC13** would be expected to display a symmetric energy landscape to interconversion, with a favorable energy well at either side and a surmountable energetic barrier separating them, **CC2** is expected to show an asymmetric energy landscape. This could explain why chiral interconversion of **CC2** does not occur at room temperature: the resultant structure is unfavorable, and would revert back to the original chirality. A computational investigation was carried out to confirm this hypothesis. **CC2** structures corresponding to different steps of the chiral interconversion were analyzed using density functional theory and their relative energies were compared (see SI, computational methods, and Figs. S11 and S12, Table S1). Results show that flipping the chirality of **CC2**-*R* but leaving all the methyl groups in the exo position leads to an extremely strained structure, which lies 135.5 kJ mol^{-1} above the initial one. Moving all the methyl groups from the *exo* to the *endo* position releases the structural strain somewhat, but still leaves the structure 45.6 kJ mol^{-1} higher than the *exo* structure of opposite chirality (Fig. 15).

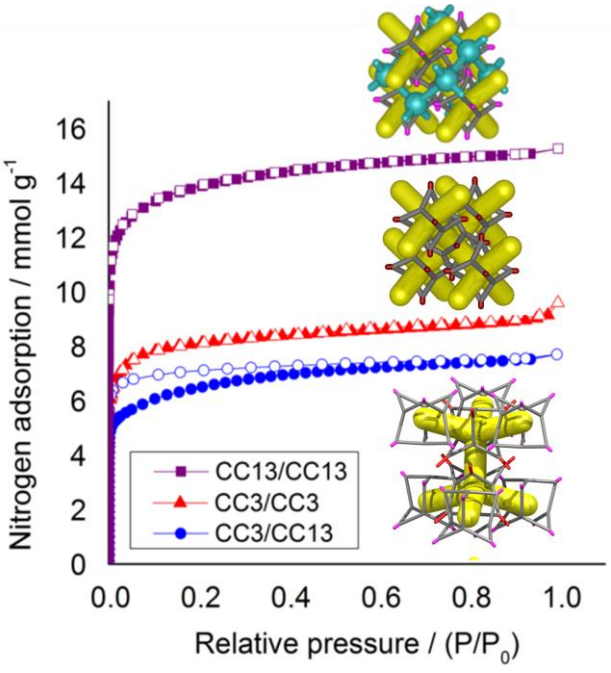

Figure 12. Nitrogen sorption isotherms (77 K, 1 bar) for racemic and quasiracemic cocrystals of **CC3** and **CC13,** all assembled in a window-window packing mode**. CC3** racemate, red triangles; (**CC3**, **CC13**) quasiracemic cocrystal blue circles, and; **CC13** racemate, green squares. Adsorption isotherms shown as solid symbols, and desorption curves as open symbols. Insets show the packing of racemic **CC13**, above, and both racemic **CC3** and **CC3**/**CC13**, below. Only the **CC13** racemate has a second interpenetrating pore channel (shown in blue), approximately doubling its porosity.

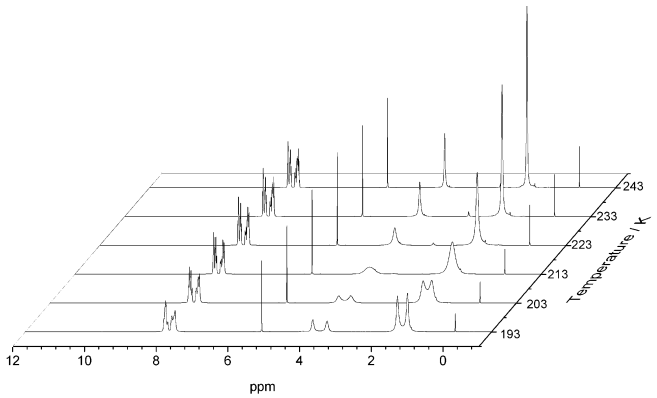

Figure 13. Variable temperature ^{1}H NMR of **CC13** recorded in CD_2Cl_2. Splitting of the peaks at 3.80 ppm (s, 1 H, N–CH2-C), and 1.51 ppm (s, 3 H, –C(CH_3)$_2$) can be observed at lower temperatures.

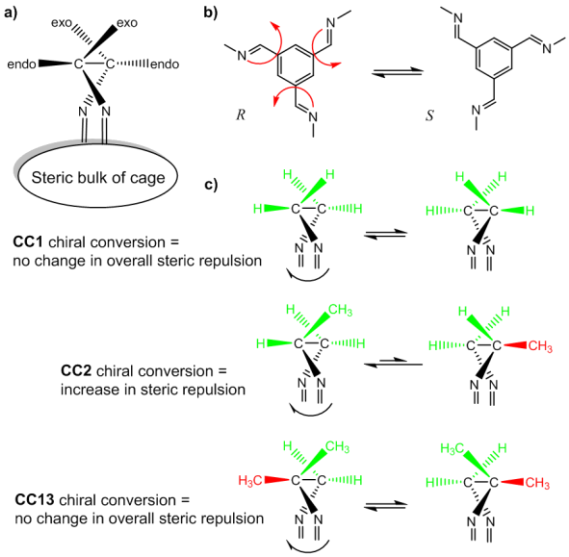

Figure 14. Schematic of **CC1**, **CC2**, and **CC13** chiral interconversion. Both **CC1** and **CC13** should exhibit symmetrical energy landscapes when interchanging from *R* to *S* chirality, whereas **CC2** favours the as-formed chirality with all methyl groups in the favourable *exo* position.

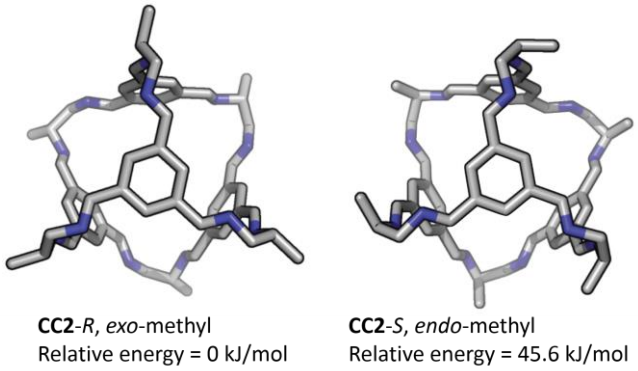

Figure 15 . Simulated structures of **CC2**-*R* with methyl groups shown in the exo position, as observed in the crystal structure, and after conversion to **CC2**-*S*, with the methyl groups moved to the *endo* position, which results in a higher relative energy.

Conclusions

A homochiral form of porous organic cage **CC2** is reported for the first time. It is possible to isolate this chiral form from a racemic **CC2** mixture by selective crystallization as well as by direct synthesis from the chiral diamine precursor. Homochiral **CC2** was found to have improved solubility, and both its crystal packing and resultant sorption properties were modified with respect to racemic **CC2**. The chirality of the **CC2** cages was also shown to strongly affect their tendency to catenate because only homochiral catenanes are formed. The synthesis of two additional cocrystal systems, **CC2**/**CC3** and **CC3**/**CC13**, illustrates the transferability of this rational design approach, although in the case of **CC3**/**CC13**, a directing solvent, dioxane, was needed to achieve an isoreticular window-to-window packing mode. Chiral interconversion occurs in solution for **CC1** and **CC13**, but not for **CC2** where the single vertex methyl groups lock the chirality in place. As the field of porous organic cages becomes more developed, the understanding of subtle relationships between factors such as chirality, crystal packing, and cage flexibility will play an increasingly important role. Moreover, the strong effect of chirality on solubility is relevant to the design of next-generation porous organic liquids, where porosity depends on producing a liquid with a high concentration of cage cavities.

Acknowledgements

We acknowledge the European Research Council under the European Union's Seventh Framework Programme (FP/2007-2013)/ERC through grant agreement n. 321156 (ERC-AG-PE5-ROBOT) and EPSRC (grants EP/N004884/1) for funding. T.H. and K.E.J. thank the Royal Society for University Research Fellowships. We acknowledge Rob Clowes for assistance with sorption measurements, Dan Holden and Rebecca Greenaway for useful discussions, and Marc Schmidtmann for preliminary crystallographic investigations. We thank Diamond Light Source for access to beamline I11 (EE12336) and I19 (MT11231) that contributed to the results presented here.

Notes and references

1. F. Schüth, K. S. W. Sing and J. Weitkamp, eds., *Handbook of Porous Solids*, Wiley VCH, Heidelberg, 2002.
2. S. Kitagawa, R. Kitaura and S. Noro, *Angew. Chem.-Int. Edit.*, 2004, **43**, 2334-2375.
3. H. M. El-Kaderi, J. R. Hunt, J. L. Mendoza-Cortes, A. P. Cote, R. E. Taylor, M. O'Keeffe and O. M. Yaghi, *Science*, 2007, **316**, 268-272.
4. Y. H. Xu, S. B. Jin, H. Xu, A. Nagai and D. L. Jiang, *Chemical Society Reviews*, 2013, **42**, 8012-8031.
5. T. Hasell and A. I. Cooper, *Nature Reviews Materials*, 2016, **1**, 16053.
6. J. Tian, P. K. Thallapally and B. P. McGrail, *CrystEngComm*, 2012, **14**, 1909-1919.
7. G. Zhang and M. Mastalerz, *Chemical Society Reviews*, 2014, **43**, 1934-1947.
8. T. Tozawa, J. T. A. Jones, S. I. Swamy, S. Jiang, D. J. Adams, S. Shakespeare, R. Clowes, D. Bradshaw, T. Hasell, S. Y. Chong, C. Tang, S. Thompson, J. Parker, A. Trewin, J. Bacsa, A. M. Z. Slawin, A. Steiner and A. I. Cooper, *Nature Materials*, 2009, **8**, 973-978.
9. M. E. Briggs and A. I. Cooper, *Chemistry of Materials*, 2017, **29**, 149-157.
10. Y. H. Jin, B. A. Voss, R. D. Noble and W. Zhang, *Angew. Chem.-Int. Edit.*, 2010, **49**, 6348-6351.
11. Y. Jin, Y. Zhu and W. Zhang, *CrystEngComm*, 2013, **15**, 1484-1499.
12. M. Mastalerz, *Angew. Chem.-Int. Edit.*, 2010, **49**, 5042-5053.
13. A. Avellaneda, P. Valente, A. Burgun, J. D. Evans, A. W. Markwell-Heys, D. Rankine, D. J. Nielsen, M. R. Hill, C. J. Sumby and C. J. Doonan, *Angew. Chem.-Int. Edit.*, 2013, **52**, 3746-3749.
14. G. Zhang, O. Presly, F. White, I. M. Oppel and M. Mastalerz, *Angewandte Chemie International Edition*, 2014, **53**, 1516-1520.
15. T. Hasell, J. L. Culshaw, S. Y. Chong, M. Schmidtmann, M. A. Little, K. E. Jelfs, E. O. Pyzer-Knapp, H. Shepherd, D. J. Adams, G. M. Day and A. I. Cooper, *Journal of the American Chemical Society*, 2014, **136**, 1438-1448.
16. J. T. A. Jones, D. Holden, T. Mitra, T. Hasell, D. J. Adams, K. E. Jelfs, A. Trewin, D. J. Willock, G. M. Day, J. Bacsa, A. Steiner and A. I. Cooper, *Angew. Chem.-Int. Edit.*, 2011, **50**, 749-753.
17. A. G. Slater, M. A. Little, PulidoA, S. Y. Chong, HoldenD, ChenL, MorganC, WuX, ChengG, ClowesR, M. E. Briggs, HasellT, K. E. Jelfs, G. M. Day and A. I. Cooper, *Nat Chem*, 2017, **9**, 17-25.
18. D. Beaudoin, F. Rominger and M. Mastalerz, *Angewandte Chemie International Edition*, 2017, **56**, 1244-1248.
19. T. Hasell, S. Y. Chong, K. E. Jelfs, D. J. Adams and A. I. Cooper, *Journal of the American Chemical Society*, 2012, **134**, 588-598.
20. T. Hasell, S. Y. Chong, M. Schmidtmann, D. J. Adams and A. I. Cooper, *Angew. Chem.-Int. Edit.*, 2012, **51**, 7154-7157.

21. L. Chen, P. S. Reiss, S. Y. Chong, D. Holden, K. E. Jelfs, T. Hasell, M. A. Little, A. Kewley, M. E. Briggs, A. Stephenson, K. M. Thomas, J. A. Armstrong, J. Bell, J. Busto, R. Noel, J. Liu, D. M. Strachan, P. K. Thallapally and A. I. Cooper, *Nat Mater*, 2014, **13**, 954-960.
22. A. Kewley, A. Stephenson, L. Chen, M. E. Briggs, T. Hasell and A. I. Cooper, *Chemistry of Materials*, 2015, DOI: 10.1021/acs.chemmater.5b01112.
23. S.-M. Xie, J.-H. Zhang, N. Fu, B.-J. Wang, L. Chen and L.-M. Yuan, *Analytica Chimica Acta*, 2016, **903**, 156-163.
24. J.-H. Zhang, S.-M. Xie, L. Chen, B.-J. Wang, P.-G. He and L.-M. Yuan, *Analytical Chemistry*, 2015, **87**, 7817-7824.
25. J.-H. Zhang, S.-M. Xie, B.-J. Wang, P.-G. He and L.-M. Yuan, *Journal of Chromatography A*, 2015, **1426**, 174-182.
26. T. Hasell, X. F. Wu, J. T. A. Jones, J. Bacsa, A. Steiner, T. Mitra, A. Trewin, D. J. Adams and A. I. Cooper, *Nature Chemistry*, 2010, **2**, 750-755.
27. J. T. A. Jones, T. Hasell, X. Wu, J. Bacsa, K. E. Jelfs, M. Schmidtmann, S. Y. Chong, D. J. Adams, A. Trewin, F. Schiffman, F. Cora, B. Slater, A. Steiner, G. M. Day and A. I. Cooper, *Nature*, 2011, **474**, 367-371.
28. K. E. Jelfs, F. Schiffmann, J. T. A. Jones, B. Slater, F. Cora and A. I. Cooper, *Physical Chemistry Chemical Physics*, 2011, **13**, 20081-20085.
29. T. Hasell, J. A. Armstrong, K. E. Jelfs, F. H. Tay, K. M. Thomas, S. G. Kazarian and A. I. Cooper, *Chemical Communications*, 2013, **49**, 9410-9412.